RAA 2017 Vol. **17** No. **6**, 62 (12pp) doi: 10.1088/1674–4527/17/6/62

http://www.raa-journal.org *http://iopscience.iop.org/raa*

***R**esearch in*
***A**stronomy and*
***A**strophysics*

Candidate members of the Pal 5, GD-1, Cetus Polar and Orphan tidal stellar halo streams from SDSS DR9, LAMOST DR3 and APOGEE catalogs

Guang-Wei Li[1], Brian Yanny[2], Hao-Tong Zhang[1], Zong-Rui Bai[1], Yue Wu[1], Yi-Qiao Dong[1], Ya-Juan Lei[1], Hai-Long Yuan[1], Yong-Hui Hou[3], Yue-Fei Wang[3] and Yong Zhang[3]

[1] Key Lab for Optical Astronomy, National Astronomical Observatories, Chinese Academy of Sciences, Beijing 100012, China; *lgw@bao.ac.cn*

[2] Fermi National Accelerator Laboratory, Batavia, IL 60510, USA

[3] Nanjing Institute of Astronomical Optics & Technology, National Astronomical Observatories, Chinese Academy of Sciences, Nanjing 210042, China

Received 2016 November 3; accepted 2017 March 20

Abstract We present candidate members of the Pal 5, GD-1, Cetus Polar and Orphan tidal stellar streams found in LAMOST DR3, SDSS DR9 and APOGEE catalogs. In LAMOST DR3, we find 20, 4 and 24 high confidence candidates of tidal streams GD-1, Cetus Polar and Orphan respectively. We also list 59, 118 and 10 high confidence candidates of tidal streams Cetus Polar, Orphan and Pal 5, respectively from the SDSS DR9 spectroscopic catalog. Furthermore, we find seven high confidence candidates of the Pal 5 tidal stream in the APOGEE data. Compared with SDSS, the new candidates from LAMOST DR3 are brighter, so that together, more of the color-magnitude diagram, including the giant branch, can be explored. Analysis of the SDSS data shows that there are three metallicity peaks associated with the Orphan stream which also exhibit some spatial separation. The LAMOST data confirm multiple metallicities in this stream. The metallicity, given by the higher resolution APOGEE instrument, of the Pal 5 tidal stream is $[\mathrm{Fe/H}] \sim -1.2$, higher than that given earlier by SDSS spectra. Many previously unidentified stream members are tabulated here for the first time, along with existing members, allowing future researchers to further constrain the orbits of these objects as they move within the Galaxy's dark matter potential.

Key words: Galaxy: structure general: stream — Galaxy: structure individual (GD-1, Orphan, Cetus, Pal 5)

1 INTRODUCTION

There are two popular models for how our Galaxy formed. The first, given by Eggen et al. (1962), suggested that the Galaxy was born from a single rapid collapse of a massive cloud of gas. Later, Searle & Zinn (1978) suggested that an inner halo may have come from a large early collapse, but the outer halo independently evolved over a much longer period of time, and during this time, many small stellar systems merged into the halo, and were tidally disrupted by the Galaxy's potential. The standard ΛCDM cosmological model also favors big galaxies growing from the merger of smaller units.

The largest and most famous Milky Way halo stellar stream is associated with the Sagittarius dwarf galaxy (Ibata et al. 1994), mapped out in 2MASS giants by Majewski et al. (2003). Much progress in stream detection occurred with the release of the SDSS dataset (York et al. 2000). Four streams: GD-1, Orphan, Cetus Polar Stream (CPS) and the Pal 5 tidal stream were discovered using SDSS data. GD-1 is a 63° narrow stream, found by Grillmair & Dionatos (2006). Later, Willett et al. (2009) fit an orbit. Yanny et al. (2009b) noticed that

there is a tidal stream near the Sgr trailing tidal tail which was named CPS by Newberg et al. (2009). Its parameters were given by Yam et al. (2013) using SDSS DR8. The Orphan stream was found by Grillmair & Dionatos (2006) and Belokurov et al. (2006), but its orbital parameters were not clear until Newberg et al. (2010) provided them using SDSS DR7. Pal 5 is a globular cluster which is being disrupted. Its long tail was firstly discovered by Odenkirchen et al. (2001), which spans more than 23° (Carlberg et al. 2012), and is the most obvious stream associated with a Galactic globular cluster.

Having an accurate census of stream members, as well as their spectroscopic properties (including radial velocity and parameters which may be used to estimate absolute magnitude – and thus distance) is crucial to determining accurate orbits of the streams. In turn, having an accurate orbit for a set of streams allows us to probe the (dark matter dominated) gravitational potential at a variety of distances and directions throughout the Milky Way's halo (Newberg et al. 2010).

A major unresolved question in Galactic dynamics is understanding in detail the shape (i.e. oblate, prolate, spherical, lumpy, changing-with-radius?) and extent (total mass and drop-off with radius) of our Galaxy's dark matter potential and the dark halo's shape and size. For instance, is the halo triaxial in nature as suggested by Law et al. (2009)? Having extensive, accurate stellar stream membership information, along with radial velocity and photometric parallax information for member stars can help resolve this important question. This work adds to our list of known stream members, with spectroscopic velocity and other stellar parameters for four halo streams.

The Large Sky Area Multi-Object Fiber Spectroscopic Telescope (LAMOST, also called the Guo Shou Jing Telescope) (Cui et al. 2012; Wang et al. 1996; Su & Cui 2004) is a special reflecting Schmidt telescope with field of view of 5° and effective aperture of 3.6 m – 4.9 m. There are 4000 fibers on its focal plane and they can record 4000 spectra at once. Its wavelength coverage is 365 nm – 900 nm with R ∼1800. Each of 16 spectrographs records images of 250 fibers on a 4136 pixel × 4160 pixel CCD. As of 2015 May 30, more than 3 million A, F, G and K stellar spectra with parameters have been released (Luo et al. 2012; Zhao et al. 2012) (see *http://dr3.lamost.org/*).

In this paper, we search for and describe parameters for high confidence stellar candidates of the GD-1, Orphan, CPS and Pal 5 tidal streams in the spectral data of LAMOST DR3, SDSS DR9 (Yanny et al. 2009a) and APOGEE (Majewski et al. 2015).

2 CANDIDATES OF STREAMS

We search for stream members, primarily giants ($0 < \log\ g < 3.5$), in the LAMOST DR3, SDSS DR9 and APOGEE spectral databases. As is common in the literature, magnitudes with subscript 0 indicate they have been corrected by the extinction given by Schlegel et al. (1998), (not the more recent Schlafly & Finkbeiner (2011) – the differences are tiny at these higher Galactic $|b|$). All g and r band magnitudes in this paper are from SDSS DR9. Because the [Fe/H] values estimated by the standard LAMOST processing pipeline (Wu et al. 2014) have a lower limit of -2.4, there is no star with quoted [Fe/H] less than -2.4 in LAMOST DR3. For SDSS stars with spectra, Newberg et al. (2009) found the quoted FEHWBG (Wilhelm et al. 1999) (WBG) parameter is a better measure of metallicity than FEHADOP for blue horizontal branch (BHB) stars, so we use WBG metallicity for stars with $(g-r)_0 < 0.2$ and FEHADOP (adopted) metallicity for stars with $(g-r)_0 > 0.2$. For a star observed many times, we only retain the spectrum with the highest signal-to-noise ratio (SNR) in the g and r bands for LAMOST spectra, and that with the highest SNR for SDSS and APOGEE. We convert radial velocities to the Galactic standard of rest velocities ($V_{\rm gsr}$) using the formula $V_{\rm gsr} = RV + 10.1\cos b\cos l + 224\cos b\sin l + 6.7\sin b$, where RV is the heliocentric radial velocity in km s^{-1}, while (l, b) is the Galactic coordinate of the star.

For each of the four streams accessible with LAMOST, SDSS or APOGEE spectroscopy, and which have SDSS g and r-band photometry, we search in the up to six-dimensional space defined by: (1,2) (l, b) position along the orbit; (3) distance (determined by photometric parallax using the cataloged star's color, magnitude and spectral type (giant or dwarf) depending on surface gravity); (4) velocity and (5,6) (lack of measureable) proper motion to select candidates and give confidence estimates of candidates' membership in a given stream. We give each candidate a number (1, 2 or 3) to describe our confidence in stream membership, with a higher number indicating lower confidence.

2.1 Candidates of the GD-1 Stream

The study of Willett et al. (2009) has given all the GD-1 stream candidates present in SDSS data, so here we only

search for GD-1 candidates in LAMOST DR3, using the same method as Willett et al. (2009). All giant candidates match the following criteria:

(1) The GD-1 positional locus is $\delta = -864.5161 + 13.22518\alpha - 0.06325544\alpha^2 + 0.0001009792\alpha^3$. Candidates should be within $\delta \pm 1^\circ$.
(2) There are seven sets (regions) of stars close in position and velocity listed in Willett et al. (2009). Regions 1, 4, 5 and 6 have high confidence stream members. Between Region 1 and Region 4, Region 2 is more reliable than Region 3 (in terms of groupings of velocities and color-magnitude properties of candidate stars), so we only use data from Region 2. Beyond Region 6, the only data we can use are from Region 7 though it is not as reliable as Regions 1, 4, 5 and 6. Thus, we use $V_{\rm gsr}$ in Regions 1, 2, 4, 5, 6 and 7 to select candidates. We generate the velocity trendline by interpolation and extrapolation of velocities of these regions, then select candidates within $30\,{\rm km\,s^{-1}}$ around the trendline.
(3) Galactic proper motions and errors are calculated from equatorial proper motions with errors in the SDSS DR9 (based on the UCAC4 catalog). We select high confidence candidates by limiting their proper motion within 2σ of the expected proper motions given by Willett et al. (2009).
(4) Metallicities [Fe/H] should be in the range $[-2.5, -1.5]$.

Figure 1 displays their metallicity distribution. As shown by figure 2 in Gao et al. (2015), LAMOST overestimates metallicities for the most metal-poor stars, and their variance is larger than that of metal-richer stars. The metallicity distribution of GD-1 member candidates from SDSS DR7, exhibited in figure 5 in Willett et al. (2009), is also broad. Thus, although these stars span a broad metallicity range, we still consider them candidate members of the GD-1 stream.

The red polygon in Figure 2 shows the area where the high confidence candidates are located. Their color-magnitude diagram (CMD, hereafter) is shown in Figure 3. We estimate their absolute magnitudes as they are giants similar to metal poor giants in the globular cluster M92, using the M92 isochrone and then remove candidate stars with implied distances far from the GD-1 stream distance. This leaves us with 20 high confidence candidates. Magnitudes of the brightest five stars, which we believe are GD-1 members, are not reliable because the SDSS CCD saturates around $r \sim 14.5$. For a stream, brighter members are fewer, so if these five bright stars really belong to the GD-1 stream, they will greatly help us to understand the stream.

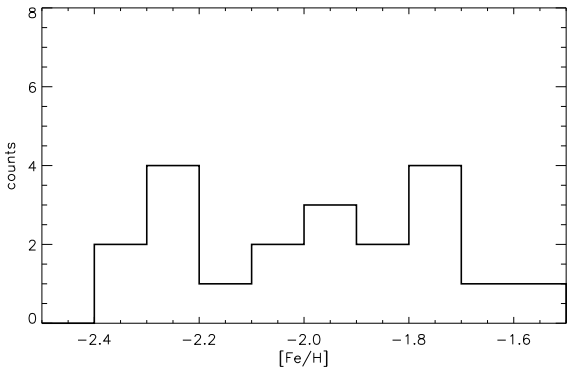

Fig. 1 The metallicity distribution of GD-1 stars in LAMOST DR3 that match all criteria.

One star in Region 1 has no SDSS photometry, but we still retain it, because there are only two candidates in Region 1. If it is really a GD-1 member, it would be valuable to study this region.

The confidence level of each candidate is given based on its position in Figure 2 and Figure 3. Let Dv_i denote the difference between $V_{\rm gsr}$ of the ith candidate and the trendline at its longitude, and $\sigma_1^2 = \sum_{i\in\phi} Dv_i^2/(n-1)$, where $\phi = \{i||Dv_i| < 3\sigma_1\}$ and n is the number of elements in ϕ; let Dc_i denote the difference between $(g-r)_0$ of the ith candidate and the M92 isochrone at its $g_{\rm corr}$, and $\sigma_2^2 = \sum_{i\in\psi} Dc_i^2/(m-1)$, where $\psi = \{i||Dc_i| < 3\sigma_2\}$ and m is the number of elements in ϕ. Then we calculate f_i for the ith candidate by the formula: $f_i = (\frac{Dv_i}{\sigma_1})^2 + (\frac{Dc_i}{\sigma_2})^2$. If $f_i \leq 2$, then the confidence level of the ith candidate is set to be 1; if $2 < f_i \leq 10$, then the confidence level is set to be 2; if $f_i > 10$, then the confidence level is set to be 3.

We searched for GD-1 candidates in APOGEE spectral data, but found none.

2.2 Candidates of the Cetus Polar Stream

We select CPS candidates by the method given by Yam et al. (2013) . All giant candidates should match the following criteria:

(1) Metallicities should be in $[-2.5, -1.5]$.
(2) Distances to the Galactic great circle $l = 143^\circ$ should be less than 15°.
(3) We find that the stream velocity formula $V_{\rm gsr} = -41.67-(0.84\times b)-(0.014\times b^2)$ given by Yam et al. (2013) has a typographical error, and the correct formula is $V_{\rm gsr} = -41.67+(0.84\times b)+(0.014\times b^2)$,

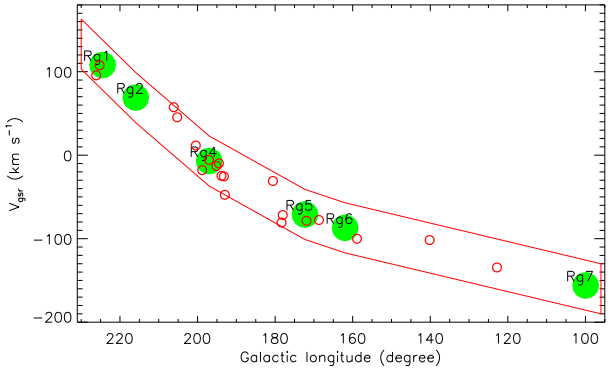

Fig. 2 Big green filled circles are $V_{\rm gsr}$ of regions given by Willett et al. (2009). The red polygon is the area where we select candidates of GD-1. The red circles are the high confidence candidates in LAMOST DR3.

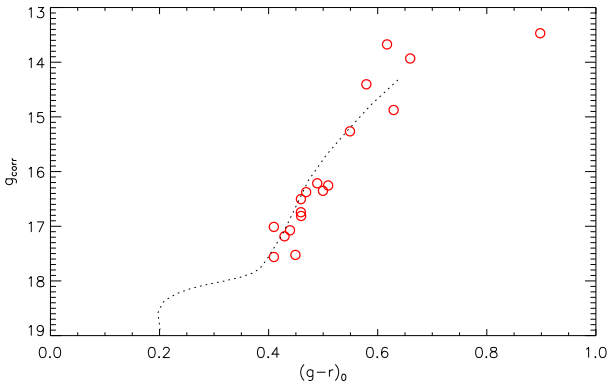

Fig. 3 The red circles are the high confidence candidates of GD-1. The background line is the M92 fiducial locus. Each candidate is corrected to the distance of M92, which is 8.2 kpc. Magnitudes of the top five stars are inaccurate due to saturation, and one star has no SDSS photometry – it is not shown in the figure.

so we use this. We select candidates within $V_{\rm sgr} \pm 20\,{\rm km\,s^{-1}}$.

(4) We use the fiducial sequence of NGC 5466 as a reference to select high confidence candidates in the CMD, then use equation 2 in Yam et al. (2013) to calculate their corrected magnitudes $g_{\rm corr}$. All stars should be within $-0.01800g_{\rm corr}^3 + 0.98473g_{\rm corr}^2 - 18.05165g_{\rm corr} + 111.43819 - 0.04 < (g-r)_0 < -0.01800g_{\rm corr}^3 + 0.98473g_{\rm corr}^2 - 18.05165g_{\rm corr} + 111.43819 + 0.04$ and $16 < g_{\rm corr} < 18.5$.

(5) Proper motions in R.A. and Dec. are all less than 6 mas yr^{-1}.

Figure 4 shows the CMD of these candidates in LAMOST DR3. The red circles are candidates we select. The stars represented by crosses are candidates, which match criteria 1, 2, 3 and 5. From Figure 5 we can see

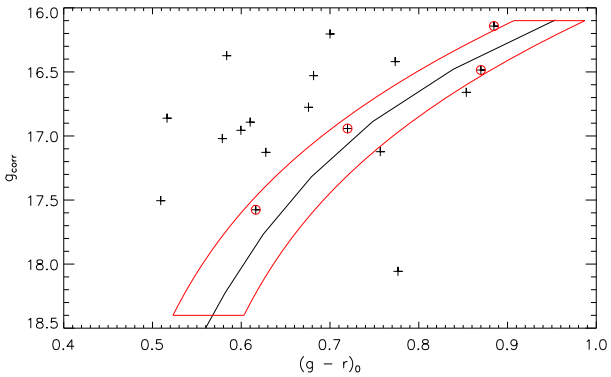

Fig. 4 This figure shows the CPS candidates in LAMOST DR3. The stars represented by crosses are those which match criteria 1, 2, 3 and 5, while the high confidence candidates are marked by red circles. The black line is the fiducial sequence of NGC 5466 shifted to the distance modulus 17.389. The area defined by criterion 4 is shown by red lines.

that the colors of brighter Orphan stars are slightly higher than the fiducial sequence of NGC 5466, so we retain the top right corner star.

Additionally, we search for additional CPS candidates within SDSS DR9 by the same criteria as above except the metallicity is restricted to $[-2.5, -2]$. Here we obtain 59 candidates, including 21 BHB stars.

Figure 5 shows the CMD of stars in the CPS area. The red diamonds in the area enclosed by red and blue lines are the high confidence candidates. While many of these objects were already shown in Yam et al. (2013), there is, displayed with red, a blue rectangle containing new candidates not identified in Yam et al. (2013).

Figure 6 exhibits the distribution range in Galactic coordinates. The central line is $l = 143°$, the two dotted lines are the $10°$ bounds from the central line on the celestial sphere, and the crosses are the candidates in SDSS DR9. From this figure we can see that the width of CPS spans $\sim 20°$, and almost all CPS candidates lie in $130° < l < 160°$ and $-25° < b < -75°$. CPS may extend beyond $l = 160°$, but this will need confirmation by another spectroscopic survey.

There are no APOGEE data available with corresponding photometric and proper motion data which overlap CPS.

Because candidates of CPS from both SDSS DR9 and LAMOST DR3 are all within narrow strips in their CMD and $V_{\rm gsr}$ figures, we are highly confident in membership, and their confidence levels are set to 1.

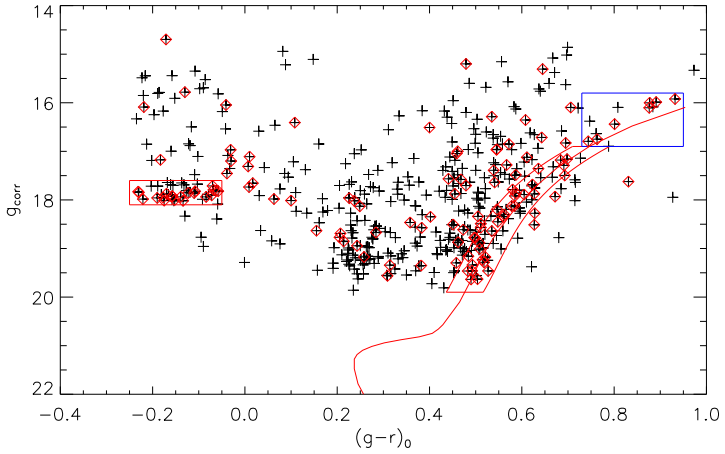

Fig. 5 The crosses are the candidates of the CPS in SDSS DR9 that match criteria 2 – 5. The red diamonds are stars with metallicity in $[-2.5, -2.0]$. The area enclosed by red and blue lines is where we select candidates. The blue rectangle is the new area not given by Yam et al. (2013).

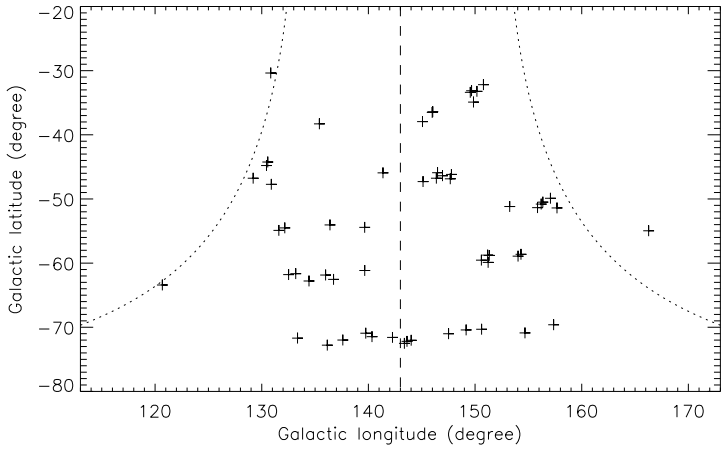

Fig. 6 This figure shows the distribution range of the CPS in Galactic coordinates. The central line is $l = 143°$, the two dotted lines are the $10°$ bounds from the central line on the celestial sphere, while the crosses are the candidates in SDSS DR9.

2.3 Candidates of the Orphan Stream

We select Orphan stream candidates by the method given by Newberg et al. (2010). In their paper, they defined a new coordinate system $(B_{\rm Orphan}, \Lambda_{\rm Orphan})$. Under this coordinate system, they defined a variable $B_{\rm corr}$ to let the stream locus be at $B_{\rm corr} = 0$. Here, we also use these symbols with the same definitions. All giant candidates should match the following criteria:

(1) Metallicities should be within $[-2.5, -1.6]$;
(2) These candidates should be within $-2° < B_{\rm corr} < 2°$.
(3) We denote $T_{\rm Orphan} = -0.0445\Lambda^2_{\rm Orphan} - 0.935\Lambda_{\rm Orphan} + 130$. Then their Galactic standard of rest velocities $V_{\rm gsr}$ are within $T_{\rm Orphan} \pm 35\,{\rm km\,s^{-1}}$.
(4) We calculate their $g_{\rm corr}$ by the formula: $g_{\rm corr} = g_0 - 0.00022\Lambda^2_{\rm Orphan} + 0.034\Lambda_{\rm Orphan}$.
(5) Proper motions in R.A. and Dec. are all less than $6\,{\rm mas\,yr^{-1}}$.
(6) We shift the isochrone of M92 to the place where its BHB is at $g_0 = 17.75$.

Figure 7 shows the CMDs of Orphan stream candidates in SDSS and LAMOST data. The left panel and the right panel are the Orphan stream CMD of SDSS candidates and LAMOST candidates respectively. In each panel, the filled circles are stars in $T_{\rm Orphan} \pm 17.5\,{\rm km\,s^{-1}}$, while open circles are stars in $T_{\rm Orphan} \pm 35\,{\rm km\,s^{-1}}$. The isochrone of M92 is shifted to have its BHB at $g_0 = 17.75$, as Newberg et al. (2010) did. In the LAMOST data, the photometry of at least four stars is unreliable.

In Figure 8, the metallicity distributions of Orphan stream candidates in SDSS and LAMOST data are shown

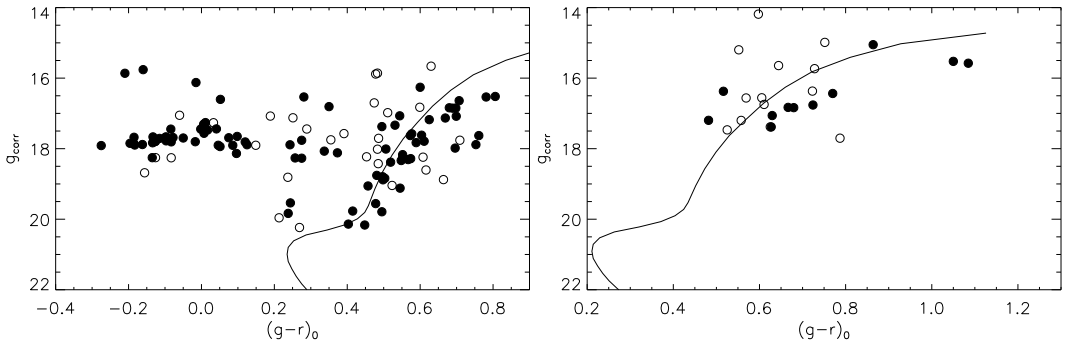

Fig. 7 The left panel and the right panel are the CMDs of Orphan stream candidates in SDSS and LAMOST data respectively. In each panel, the filled circles are stars within $T_{\rm Orphan} \pm 17.5\,{\rm km\,s^{-1}}$, while open circles are stars within $T_{\rm Orphan} \pm 35\,{\rm km\,s^{-1}}$. In each panel, the isochrone of M92 is shifted to have its BHB at $g_0 = 17.75$.

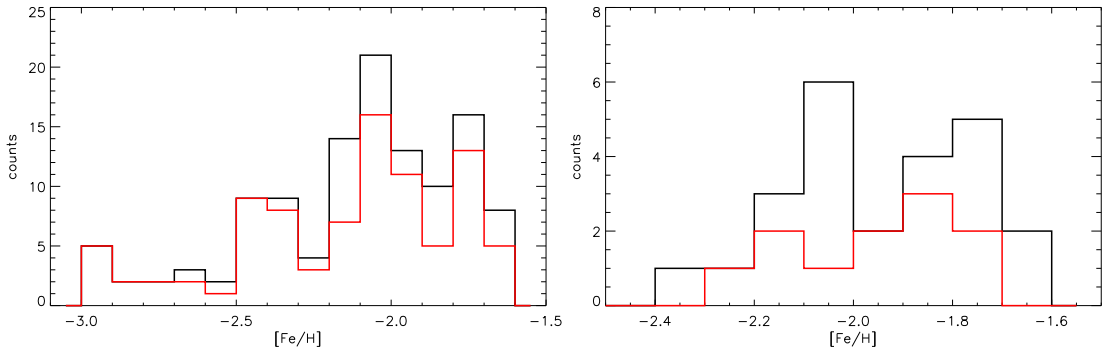

Fig. 8 The left panel and the right panel are the metallicity distributions of Orphan stream candidates in SDSS and LAMOST data respectively. In each panel, the red histogram is the metallicity distribution of stars within $T_{\rm Orphan} \pm 17.5\,{\rm km\,s^{-1}}$, while the black histogram is for stars within $T_{\rm Orphan} \pm 35\,{\rm km\,s^{-1}}$.

respectively by the left and right panels. In each panel, the red histogram is the metallicity distribution of stars in $T_{\rm Orphan} \pm 17.5\,{\rm km\,s^{-1}}$, while the black histogram is that of stars in $T_{\rm Orphan} \pm 35\,{\rm km\,s^{-1}}$. We find that for SDSS candidates, there are three metallicity peaks which are $[-2.5, -2.3]$, $[-2.2, -1.9]$ and $[-1.9, -1.6]$. The last two peaks are confirmed by LAMOST data. Because LAMOST metallicity is cutoff by $[{\rm Fe/H}] = -2.4$, the most metal-poor component does not appear in the LAMOST data. If these three metallicity peaks are real, it suggests that there are two-three components in the Orphan stream or that other stellar populations from other objects are overlapping in space and velocity.

Figure 9 shows the $V_{\rm gsr}$ of SDSS candidates along the $\Lambda_{\rm Orphan}$. The dash-dotted lines are $T_{\rm Orphan} \pm 17.5\,{\rm km\,s^{-1}}$, while the dashed lines are $T_{\rm Orphan} \pm 35\,{\rm km\,s^{-1}}$. The stars with metallicity in $[-2.5, -2.3]$, $[-2.2, -1.9]$ and $[-1.9, -1.6]$ are marked by red, green and blue circles, respectively. From Figure 9 we can see that compared to the stars with [Fe/H] in $[-2.2, -1.9]$ and $[-1.9, -1.6]$, almost all stars within the most metal-poor peak have $\Lambda_{\rm Orphan} < 0$, with only two stars in $\Lambda_{\rm Orphan} > 0$. This special metallicity pattern along the $\Lambda_{\rm Orphan}$ must relate to the origin and evolution histories of the stream, and needs further study.

There is no APOGEE star candidate in the Orphan stream.

We use similar formulas in Section 2.1 to calculate confidence levels. Let Dv_i denote the difference between $V_{\rm gsr}$ of the ith candidate and the trendline $-0.0445\Lambda^2_{\rm Orphan} - 0.935\Lambda_{\rm Orphan} + 130\,{\rm km\,s^{-1}}$ at its $\Lambda_{\rm Orphan}$, and $\sigma_1^2 = \sum_{i\in\phi} Dv_i^2/(n-1)$, where $\phi = \{i||Dv_i| < 3\sigma_1\}$ and n is the number of the elements in ϕ; let Dc_i denote the difference between $(g-r)_0$ of the ith candidate and the M92 isochrone at its $g_{\rm corr}$, and $\sigma_2^2 = \sum_{i\in\psi} Dc_i^2/(m-1)$, where $\psi = \{i||Dc_i| < 3\sigma_2\}$ and m is the number of elements in ϕ. Then we calculate the f_i for the ith candidate by the formula: $f_i = (\frac{Dv_i}{\sigma_1})^2 + (\frac{Dc_i}{\sigma_2})^2$. If $f_i \leq 2$, then the confidence level of the ith candidate is set to be 1; if $2 < f_i \leq 10$, then

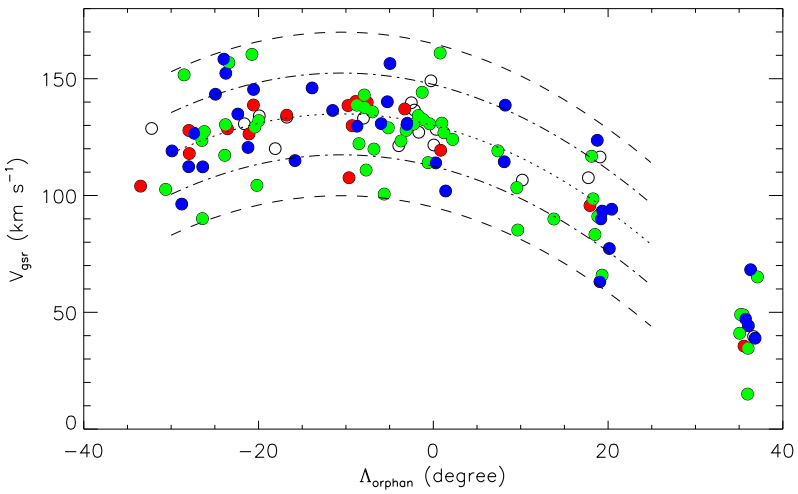

Fig. 9 This figure shows the $V_{\rm gsr}$ of SDSS candidates along $\Lambda_{\rm Orphan}$. The dash-dotted lines are $T_{\rm Orphan} \pm 17.5\,{\rm km\,s^{-1}}$, while the dashed lines are $T_{\rm Orphan} \pm 35\,{\rm km\,s^{-1}}$. The central dotted line is $T_{\rm Orphan}\,{\rm km\,s^{-1}}$. All candidates are marked by circles, while stars with [Fe/H] in $[-2.5, -2.3]$, $[-2.2, -1.9]$ and $[-1.9, -1.6]$ are marked by red, green and blue circles, respectively.

the confidence level is set to be 2; if $f_i > 10$, then the confidence level is set to be 3.

2.4 Pal 5 Tidal Stream

We select Pal 5 tidal stream candidates following the criteria from Kuzma et al. (2015). All giant candidates satisfy the following criteria:

(1) Three positions $(226.3°, -2.9°)$, $(246°, 7.9°)$ and Pal 5 center $(229°, -0.11°)$ in (RA, Dec) in Grillmair & Dionatos (2006) and the 11 centers of fields given in Table 1 by Kuzma et al. (2015) are used to calculate the trace of the Pal 5 tidal stream. First, these positions are classified into two groups: the southern group consists of the cluster center and positions to the south; the northern group consists of the cluster center and positions to the north. Then these positions in each group are converted from (RA, Dec) to (l, b). For the trailing tail (northern part of the stream), we fit positions with a cubic polynomial, which is $b = 45.9816 - 0.0250988 * l - 0.0244554 * l^2 + 0.000332027 * l^3$. For the leading tail (southern part of the stream), we fit positions by a line, $b = 45.920122 - 0.010919619 * l$. All candidates should be within $1°$ of this locus.
(2) We use photometry of stars within $8.3'$ of Pal 5's cluster center to generate a Pal 5 CMD.
(3) Proper motions in R.A. and Dec. are all less than 6 mas yr^{-1}.
(4) Metallicities are within $-2.5 <$[Fe/H] < -0.6. As RR Lyraes are variables, it is hard to get their real metallicity from one spectrum without knowing a phase. Thus, the metallicity criterion is extended to -2. Second, there are very few (or even no) candidates in these three catalogs on the long trailing tail of Pal 5, so every candidate is very valuable. We extend the metallicity criterion to –0.6. In fact, only one member candidate (a red giant) has [Fe/H]~ -0.75, while the other red giant candidates have [Fe/H] within about -1.4 ± 0.4.
(5) As mentioned by Kuzma et al. (2015), the velocity gradient along the trace is $1.0 \pm 0.1\,{\rm km\,s^{-1}\,deg^{-1}}$, so we use $RV_{\rm corr} = RV - a$ to select candidates, where a is angular distance in degree to the cluster center; $a < 0$ is for leading tail stars, $a > 0$ is for trailing tail stars and RV is the line of sight velocity. $RV_{\rm corr}$ should be within $[-70, -45]\,{\rm km\,s^{-1}}$.
(6) We use $0.00361996 g_0^3 - 0.173359 g_0^2 + 2.61828 g_0 - 11.471$ to fit the fiducial sequence of the Pal 5 red giant branch given by An et al. (2008), and use the criteria $0.00361996 g_0^3 - 0.173359 g_0^2 + 2.61828 g_0 - 11.471 + 0.1 < (g-r)_0 < 0.00361996 g_0^3 - 0.173359 g_0^2 + 2.61828 g_0 - 11.471 - 0.15, 16 < g_0 < 19.5$ and $-2 <$[Fe/H] < -0.6 to select candidates in the red and asymptotic giant branches. In the horizontal branch and RR Lyrae strip, we use the criteria $-0.3 < (g-r)_0 < 0.3$ and $16.7 < g_0 < 18.5$.

Table 1 Candidates in LAMOST

Stream	Obs ID [a]	Subclass	RA (deg)	Dec (deg)	rv [b] ($\mathrm{km\,s^{-1}}$)	$T_{\rm eff}$ (K)	[Fe/H]	$\log g$	rv_err ($\mathrm{km\,s^{-1}}$)	$T_{\rm eff}$_err (K)	[Fe/H]_err	$\log g$_err	level [c]
(1)	(2)	(3)	(4)	(5)	(6)	(7)	(8)	(9)	(10)	(11)	(12)	(13)	(14)
GD1	196716136	G5	125.22538757	–2.78869820	253.37	5001.74	–1.78	2.32	29.10	186.84	0.29	1.08	3
GD1	187405120	G7	137.72410583	21.93488503	135.74	4459.66	–1.55	1.41	48.83	344.33	0.61	1.21	3
GD1	132513055	G0	139.29585266	23.10439491	119.02	5212.79	–1.86	2.86	42.48	211.86	0.37	1.16	3
GD1	313108245	K3	125.95130157	–1.41831505	261.85	4246.94	–1.74	0.55	17.33	64.31	0.09	0.29	3
GD1	343405145	G3	155.50750732	41.43789673	–75.93	4489.56	–1.98	0.88	20.57	61.48	0.10	0.37	1
GD1	136814012	F2	153.97523499	40.22281265	–29.44	5034.87	–2.21	2.36	48.94	266.52	0.47	1.21	2
GD1	31709120	G3	153.46257019	41.59279633	–84.04	4815.06	–1.64	1.86	25.35	250.98	0.41	1.10	2
GD1	19114174	G0	143.17625427	28.68422318	33.63	4878.86	–2.24	1.86	47.26	216.92	0.36	1.08	1
GD1	196716136	G5	125.22538757	–2.78869820	253.37	5001.74	–1.78	2.32	29.10	186.84	0.29	1.08	3
GD1	187405120	G7	137.72410583	21.93488503	135.74	4459.66	–1.55	1.41	48.83	344.33	0.61	1.21	3
GD1	132513055	G0	139.29585266	23.10439491	119.02	5212.79	–1.86	2.86	42.48	211.86	0.37	1.16	3
GD1	313108245	K3	125.95130157	–1.41831505	261.85	4246.94	–1.74	0.55	17.33	64.31	0.09	0.29	3
GD1	343405145	G3	155.50750732	41.43789673	–75.93	4489.56	–1.98	0.88	20.57	61.48	0.10	0.37	1
GD1	136814012	F2	153.97523499	40.22281265	–29.44	5034.87	–2.21	2.36	48.94	266.52	0.47	1.21	2
GD1	31709120	G3	153.46257019	41.59279633	–84.04	4815.06	–1.64	1.86	25.35	250.98	0.41	1.10	2
GD1	19114174	G0	143.17625427	28.68422318	33.63	4878.86	–2.24	1.86	47.26	216.92	0.36	1.08	1
GD1	144415133	F2	145.67654419	32.36338043	11.76	4919.19	–2.33	2.03	45.05	298.79	0.46	1.20	1
GD1	20205027	G0	166.01896667	49.15338516	–141.72	5067.95	–2.25	2.36	35.05	295.35	0.45	1.21	2
GD1	26201048	G3	177.37100220	55.62288666	–176.52	4995.78	–2.04	2.41	41.83	329.16	0.52	1.23	1
GD1	301103170	F2	160.02476501	45.67606735	–101.32	5191.97	–1.96	2.57	31.19	205.94	0.32	0.95	1
GD1	31316164	F5	144.91429138	31.43951225	27.40	5421.83	–1.86	3.19	41.28	329.40	0.54	1.01	1
GD1	177412045	F2	144.80642700	30.12451935	39.76	5232.35	–2.00	3.00	32.19	332.33	0.52	1.06	1
GD1	22612126	F6	146.28292847	32.97006607	–13.60	5118.60	–2.01	2.68	42.82	421.01	0.61	1.15	2
GD1	33215201	K3	192.98162842	57.51427460	–232.69	5398.19	–1.76	3.44	55.06	390.25	0.69	1.22	1
GD1	19110094	F5	142.15020752	27.33783531	68.58	5147.92	–2.38	2.45	63.41	402.39	0.64	1.26	1
GD1	33101141	F5	157.29130554	44.57644653	–95.99	5288.58	–2.27	3.15	34.97	304.67	0.48	0.98	1
GD1	22613170	F2	146.83998108	32.02341843	27.47	5207.86	–1.73	2.97	35.35	378.50	0.57	0.99	2
GD1	188205199	F2	146.10885620	32.80860901	9.13	5337.79	–2.13	3.07	44.52	263.22	0.46	1.20	1
Cetus	174603094	G3	20.12708660	–2.32050160	–89.16	4867.15	–2.11	1.92	38.89	321.60	0.54	1.24	1
Cetus	173415204	G2	21.11022000	–0.73523990	–89.90	4773.38	–1.97	1.74	31.14	304.59	0.48	1.22	1
Cetus	203416074	G3	20.59927750	–0.44091910	–83.35	4476.76	–2.06	0.95	28.49	222.75	0.32	0.76	1
Cetus	202113113	K3	29.15201950	27.61567690	–185.20	4382.64	–1.82	0.89	23.31	127.46	0.21	0.68	1
Orphan	336614154	G2	164.07878113	–2.87435389	204.73	5153.20	–1.80	2.72	28.12	247.77	0.37	1.01	1
Orphan	335102079	G2	163.75819397	–1.65851295	254.80	4498.49	–2.00	0.96	21.68	95.27	0.14	0.41	2
Orphan	206805239	G2	164.54008484	–0.95315701	194.14	4875.89	–2.11	1.94	36.32	141.33	0.25	1.11	2
Orphan	335110239	G7	163.70819092	–0.24515900	237.45	4627.19	–1.96	1.31	21.92	149.98	0.20	0.61	1
Orphan	21302156	G7	161.29702759	0.69140798	249.21	4911.87	–1.74	2.08	30.26	194.49	0.31	1.10	1
Orphan	202414146	G7	159.65242004	3.60706711	261.47	4971.93	–1.65	2.43	32.78	308.42	0.45	1.17	2
Orphan	338101182	G2	160.22813416	3.76154089	231.97	5201.56	–1.79	3.23	52.81	396.53	0.61	1.24	1
Orphan	215114076	G2	158.33589172	6.72535706	198.85	4950.51	–1.76	2.00	31.98	288.94	0.47	1.14	2
Orphan	215116079	G2	158.17124939	7.12918377	219.79	4756.04	–1.87	1.53	24.58	272.09	0.44	1.07	1
Orphan	338115044	G0	159.86143494	7.20790005	217.40	5230.38	–1.84	2.85	34.29	220.05	0.33	1.05	1
Orphan	338116036	K0	158.44303894	7.98268223	208.58	4702.56	–2.00	1.52	31.14	231.38	0.30	0.80	1
Orphan	338111124	G3	160.02001953	8.00695133	207.50	4713.99	–2.01	1.26	23.75	159.99	0.24	0.63	1
Orphan	280810047	G8	160.66064453	9.45373631	208.71	4738.74	–1.93	1.52	22.51	133.78	0.19	0.68	1
Orphan	221306019	G0	154.61956787	12.59383869	192.45	4965.23	–2.03	2.19	42.83	269.98	0.46	1.21	2
Orphan	226810023	G2	154.76403809	17.20409203	208.60	4695.52	–2.10	1.38	29.05	269.90	0.41	1.01	1
Orphan	105511059	G3	152.72105408	20.20342064	206.16	4667.65	–1.85	1.33	26.90	245.29	0.40	0.95	1
Orphan	139704138	G2	150.22201538	23.61906433	220.38	4932.99	–1.65	2.12	27.48	126.60	0.22	1.01	1
Orphan	307601145	G0	154.33709717	23.70523453	163.88	5116.91	–1.75	2.54	26.97	177.00	0.27	0.95	2
Orphan	213805101	K3	153.35395813	27.59321022	156.52	4514.48	–2.37	1.13	60.38	348.60	0.44	1.01	2
Orphan	188207023	K3	148.60426331	31.90862656	173.84	4812.29	–2.23	1.62	32.85	271.62	0.43	1.11	1
Orphan	188209138	G2	149.12370300	33.80524826	163.02	4904.74	–2.19	2.06	40.15	336.57	0.51	1.24	1
Orphan	307501248	G2	147.59558105	35.55714417	172.57	4529.00	–2.09	0.91	23.87	114.93	0.16	0.47	3
Orphan	342409099	G5	144.96539307	37.18752289	138.96	4258.84	–1.71	0.50	14.87	55.13	0.08	0.26	2
Orphan	121603166	G1	145.71481323	45.16758728	106.31	4223.91	–2.16	0.25	23.25	179.25	0.21	0.41	2

Notes: [a] Observation ID: the same object in different observation has different obsid which is unique for all LAMOST spectra; [b] Heliocentric velocity; [c] The confidence level: 1 represents highest confidence. Only a portion of the table is shown here for illustration. The whole table containing information on 48 stream candidates in LAMOST is available on *http://www.raa-journal.org/docs/Supp/20160222table1.txt*.

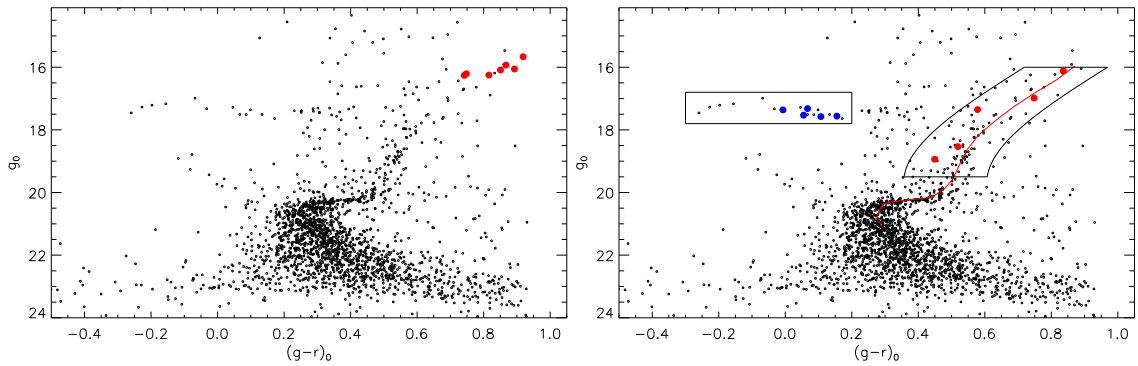

Fig. 10 *Left panel*: the CMD of APOGEE candidates in the Pal 5 tidal stream; *right panel*: the CMD of SDSS candidates in the Pal 5 tidal stream. In each panel, the background stars are within $8.3'$ of Pal 5's cluster center. Red circles are red giants, while blue circles are RR Lyraes. In the right panel, areas enclosed by black lines are where we select candidates in SDSS DR9, while the red line is the fiducial sequence of Pal 5 given by An et al. (2008).

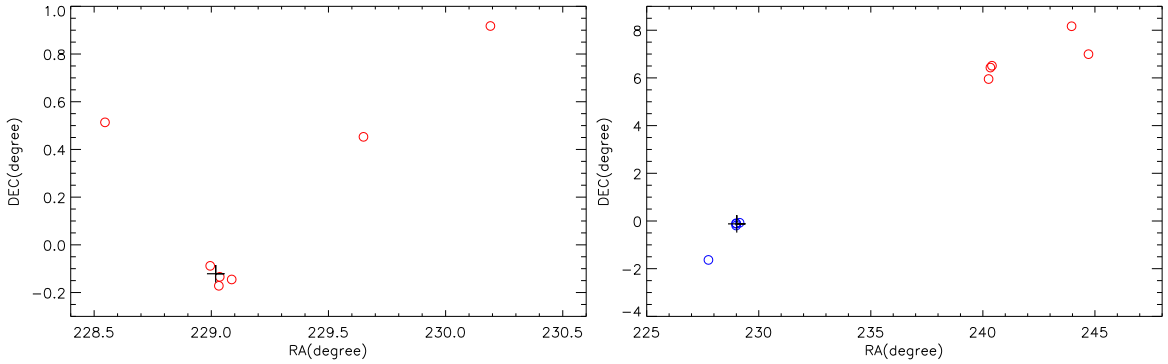

Fig. 11 *Left panel*: APOGEE candidate positions; *right panel*: SDSS candidate positions. Red circles are red giants, while blue circles are RR Lyres. A black cross in each panel is Pal 5's cluster center.

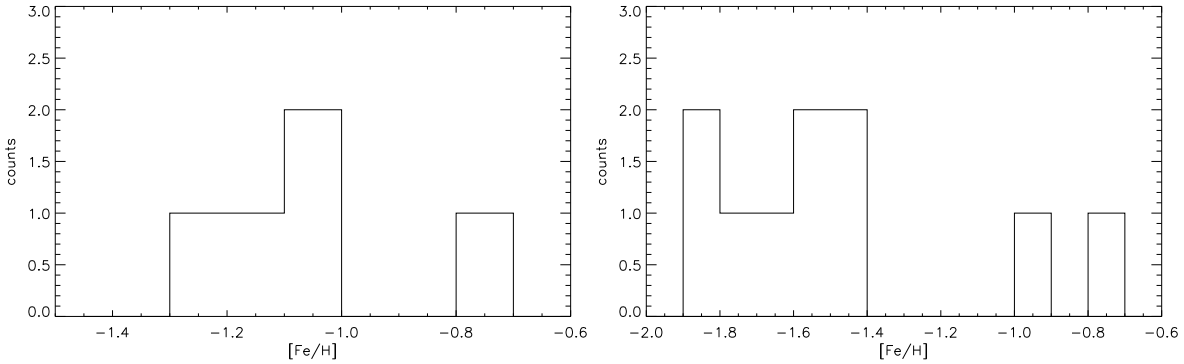

Fig. 12 *Left panel*: Metallicity distribution of Pal 5 candidates in APOGEE; *right panel*: Metallicity distribution of Pal 5 candidates in SDSS DR9.

We find no candidate in LAMOST data, but we find eight red giants in APOGEE. We also find five RR Lyraes and five red giants in the SDSS DR9 spectra.

Figures 10, 11, 12 and 13 are CMD, position, metallicity and line of sight velocity distributions respectively of Pal 5 candidates in APOGEE and SDSS DR9. From these figures, we can see APOGEE candidates are near the tip of the red giant branch, mostly near the Pal 5 core; SDSS candidates are red giants and RR Lyraes. These SDSS red giants are far from the center while RR Lyraes are near the Pal 5 cluster center. Metallicities of APOGEE candidates are around -1.1,

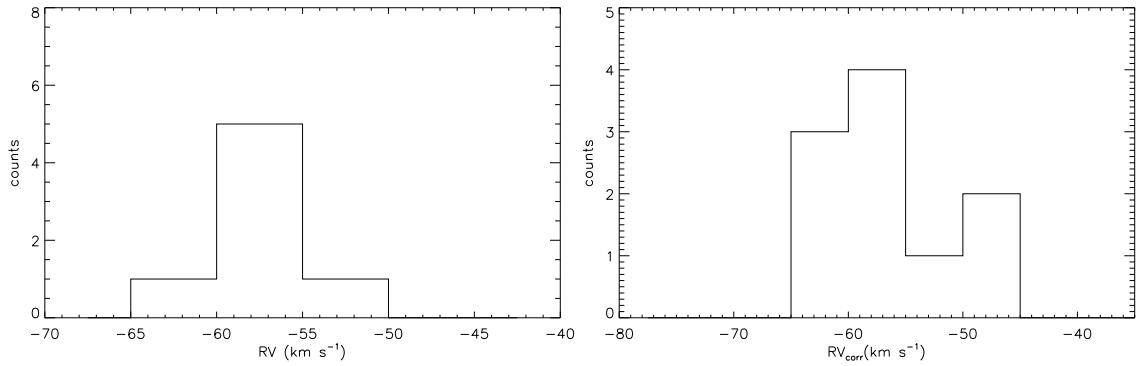

Fig. 13 *Left panel*: line of sight velocity distribution of APOGEE candidates. Because APOGEE candidates all are around Pal 5's cluster center, corrected velocity is not used. *Right panel*: Corrected velocity distribution of SDSS candidates.

Table 2 Candidates in SDSS

Stream	Plate	mjd	Fiberid	Subclass	RA (deg)	Dec (deg)	rv^a (km s^{-1})	$T_{\rm eff}$ (K)	[Fe/H]	FEHWBG	log g	rv_err (km s^{-1})	$T_{\rm eff}$_err (K)	[Fe/H]_err	FEHWBG_err	log g_err	level^b
(1)	(2)	(3)	(4)	(5)	(6)	(7)	(8)	(9)	(10)	(11)	(12)	(13)	(14)	(15)	(16)	(17)	(18)
Cetus	2864	54467	91	F9	18.992146	–10.615119	–61.74	4868.47	–2.16		1.62	1.62	55.22	0.06		0.14	1
Cetus	2878	54465	59	A0p	22.955864	–10.540712	–51.03	8456.75	–2.10	–2.10	3.39	7.31	141.34	0.29	0.29	0.29	1
Cetus	2864	54467	49	A0	19.162479	–10.344024	–54.14	7878.93	–1.72	–2.46	3.03	4.75	102.53	0.06	0.14	0.27	1
Cetus	3109	54833	111	F9	16.801901	–10.321400	–60.38	4473.98	–2.28		1.26	1.53	151.87	0.03		0.13	1
Cetus	2864	54467	102	G2	19.334705	–10.221816	–68.46	5151.40	–2.13		1.97	3.39	45.32	0.03		0.11	1
Cetus	2865	54503	269	G2	24.394780	–9.886655	–65.46	5153.11	–2.40		2.24	3.58	59.23	0.05		0.22	1
Cetus	2878	54465	312	A0p	20.752808	–9.660568	–73.00	8294.23	–1.92	–2.42	3.25	8.20	144.40	0.16	0.28	0.07	1
...	.....																

Notes: ^{a} Heliocentric velocity. ^{b} The confidence level: the lower the number, the higher the confidence. Only a portion of the table is shown here for illustration. The whole table containing information on 187 stream candidates in SDSS is available on *http://www.raa-journal.org/docs/Supp/20160222table2.txt*.

Table 3 Candidates in APOGEE

Stream	ID	RA (deg)	Dec (deg)	rv^a (km s^{-1})	$T_{\rm eff}$ (K)	[Fe/H]	log g	rv_err (km s^{-1})	$T_{\rm eff}$_err (K)	[Fe/H]_err	log g_err	level^b
(1)	(2)	(3)	(4)	(5)	(6)	(7)	(8)	(9)	(10)	(11)	(12)	(13)
Pal 5	2M15160773–0010183	229.032225	–0.171773	–58.11	5119.35	–0.79	1.98	0.38	91.47	0.05	0.11	1
Pal 5	2M15162090–0008426	229.087113	–0.145193	–57.70	4408.65	–1.09	1.12	0.16	91.47	0.05	0.11	1
Pal 5	2M15160866–0008031	229.036088	–0.134211	–64.40				0.30				1
Pal 5	2M15155888–0005171	228.995349	–0.088101	–56.77	4400.08	–1.25	0.87	0.12	91.47	0.05	0.11	1
Pal 5	2M15183589+0027100	229.649545	0.452789	–57.41	4584.16	–1.07	1.94	0.10	91.47	0.05	0.11	1
Pal 5	2M15141111+0030487	228.546300	0.513550	–54.43				4.27				1
Pal 5	2M15204588+0055032	230.191207	0.917572	–56.09	4494.36	–1.18	1.27	0.09	91.47	0.05	0.11	1

Notes: ^{a} Heliocentric heliocentric velocity. ^{b} The confidence level: 1 indicates highest confidence.

higher than -1.48 ± 0.10 dex given by Kuzma et al. (2015) and -1.41 given by the Harris catalog. The metallicity of SDSS candidates should be within $[-1.9, -1.4]$, as shown in the left panel of Figure 12, which is lower than those given by APOGEE, Kuzma et al. (2015) and the Harris catalog. For the line-of-sight velocity, its distribution of APOGEE candidates is very narrow which confirms that Pal 5 is a cool stream, though the SDSS distribution is broader.

As the APOGEE candidates and SDSS RR Lyraes are all in the Pal 5 cluster, they are bona fide members, and their confidence levels are set to 1. The five SDSS red

giants are all far from the Pal 5 center, so their confidence levels are set to 2.

3 CONCLUSIONS AND DISCUSSION

In this paper, we present three tables of high confidence candidate stellar members of the GD-1, CPS, Orphan and Pal 5 tidal streams from LAMOST DR3, SDSS DR9 and APOGEE spectroscopic catalogs. In LAMOST DR3, we find 20, 4 and 24 high confidence candidates of the GD-1 stream, CPS and Orphan stream, respectively. In SDSS DR9, we find 59, 118 and 10 high confidence candidates of CPS, Orphan stream and Pal 5 tidal stream, respectively. In APOGEE, we find seven Pal 5 high confidence candidates.

Table 1 lists the LAMOST DR3 candidates, including ID, position, spectral type, radial velocity, [Fe/H], $\log g$, $T_{\rm eff}$ and their associated errors. Table 2 lists the SDSS data, including plate, mjd, fiberid, position, spectral type, radial velocity, [Fe/H], FEHWBG, log g, $T_{\rm eff}$ and their associated errors. Table 3 gives the information for each APOGEE candidate, including ID, position, and radial velocity, $T_{\rm eff}$, [Fe/H] and $\log g$ with their errors. The last columns in these three tables show the confidence level (described by 1, 2 and 3) of each candidate, with a higher number indicating lower confidence.

Of note:

(1) The brightest stars of GD-1 and Orphan streams are all from LAMOST data, so the LAMOST data supplement the bright end of these streams.
(2) LAMOST and SDSS Orphan stream data show that there may be two or three metallicity peaks, and the most metal-poor peak is located at $\Lambda_{\rm Orphan} < 0$. Alternatively, there may be stars from other streams or coherent background or foreground halo structures in this direction on the sky. The Orphan stream may span a broader area for regions beyond $\Lambda_{\rm Orphan} < -20^\circ$ and $\Lambda_{\rm Orphan} > 10^\circ$.
(3) The cataloged APOGEE metallicity for Pal 5 is around -1.2 which is significantly higher than that given by the globular cluster and SDSS literature which quote $[{\rm Fe/H}] \sim -1.4$. APOGEE spectra are obtained with a high resolution infrared spectrograph and measure elements besides iron, magnesium or calcium to determine metallicity.

In the future, we plan to continue to probe the abundances of stream stars, including searches for gradients in abundance along the streams, in order to better understand the streams' formation and evolution histories.

Finally, we hope to use these additional candidate stream stars' velocity, metallicity and membership information to improve models of stream orbits. A fit of the four orbits simultaneously to a single Milky Way potential can then be used to constrain the potential significantly better than fitting any single stream by itself and help resolve remaining questions about the extent and shape of our dark matter halo (Newberg et al. 2010; Willett et al. 2009; Law et al. 2009).

Acknowledgements This research is supported by the National Natural Science Foundation of China (NSFC, Grant Nos. Y011161001, 11403056, 11673036 and 11333004). Support was provided by the US NSF LAMOST-PLUS grant. Y. Wu acknowledges the fund supplied by the Guangdong Provincial Engineering Technology Research Center for Data Science. We also thank the referee for valuable advice.

The Guo Shou Jing Telescope (the Large Sky Area Multi-Object Fiber Spectroscopic Telescope LAMOST) is a National Major Scientific Project built by the Chinese Academy of Sciences. Funding for the project has been provided by the National Development and Reform Commission. LAMOST is operated and managed by National Astronomical Observatories, Chinese Academy of Sciences.

References

An, D., Johnson, J. A., Clem, J. L., et al. 2008, ApJS, 179, 326
Belokurov, V., Zucker, D. B., Evans, N. W., et al. 2006, ApJ, 642, L137
Carlberg, R. G., Grillmair, C. J., & Hetherington, N. 2012, ApJ, 760, 75
Cui, X.-Q., Zhao, Y.-H., Chu, Y.-Q., et al. 2012, RAA (Research in Astronomy and Astrophysics), 12, 1197
Eggen, O. J., Lynden-Bell, D., & Sandage, A. R. 1962, ApJ, 136, 748
Gao, H., Zhang, H.-W., Xiang, M.-S., et al. 2015, RAA (Research in Astronomy and Astrophysics), 15, 2204
Grillmair, C. J., & Dionatos, O. 2006, ApJ, 643, L17
Ibata, R. A., Gilmore, G., & Irwin, M. J. 1994, Nature, 370, 194
Kuzma, P. B., Da Costa, G. S., Keller, S. C., & Maunder, E. 2015, MNRAS, 446, 3297

Law, D. R., Majewski, S. R., & Johnston, K. V. 2009, ApJ, 703, L67
Luo, A.-L., Zhang, H.-T., Zhao, Y.-H., et al. 2012, RAA (Research in Astronomy and Astrophysics), 12, 1243
Majewski, S. R., Skrutskie, M. F., Weinberg, M. D., & Ostheimer, J. C. 2003, ApJ, 599, 1082
Majewski, S. R., Schiavon, R. P., Frinchaboy, P. M., et al. 2015, arXiv:1509.05420
Newberg, H. J., Yanny, B., & Willett, B. A. 2009, ApJ, 700, L61
Newberg, H. J., Willett, B. A., Yanny, B., & Xu, Y. 2010, ApJ, 711, 32
Odenkirchen, M., Grebel, E. K., Rockosi, C. M., et al. 2001, ApJ, 548, L165
Schlafly, E. F., & Finkbeiner, D. P. 2011, ApJ, 737, 103
Schlegel, D. J., Finkbeiner, D. P., & Davis, M. 1998, ApJ, 500, 525
Searle, L., & Zinn, R. 1978, ApJ, 225, 357
Su, D.-Q., & Cui, X.-Q. 2004, ChJAA (Chin. J. Astron. Astrophys.), 4, 1
Wang, S.-G., Su, D.-Q., Chu, Y.-Q., Cui, X., & Wang, Y.-N. 1996, Appl. Opt., 35, 5155
Wilhelm, R., Beers, T. C., & Gray, R. O. 1999, AJ, 117, 2308
Willett, B. A., Newberg, H. J., Zhang, H., Yanny, B., & Beers, T. C. 2009, ApJ, 697, 207
Wu, Y., Du, B., Luo, A., Zhao, Y., & Yuan, H. 2014, in IAU Symposium, 306, Statistical Challenges in 21st Century Cosmology, eds. A. Heavens, J.-L. Starck, & A. Krone-Martins, 340
Yam, W., Carlin, J. L., Newberg, H. J., et al. 2013, ApJ, 776, 133
Yanny, B., Rockosi, C., Newberg, H. J., et al. 2009a, AJ, 137, 4377
Yanny, B., Newberg, H. J., Johnson, J. A., et al. 2009b, ApJ, 700, 1282
York, D. G., Adelman, J., Anderson, Jr., J. E., et al. 2000, AJ, 120, 1579
Zhao, G., Zhao, Y.-H., Chu, Y.-Q., Jing, Y.-P., & Deng, L.-C. 2012, RAA (Research in Astronomy and Astrophysics), 12, 723